Hindawi
International Journal of Chemical Engineering
Volume 2022, Article ID 7899996, 20 pages
https://doi.org/10.1155/2022/7899996

Research Article

Valorization of Waste Cooking Oil into Biodiesel via *Bacillus stratosphericus* Lipase Amine-Functionalized Mesoporous SBA-15 Nanobiocatalyst

Abdallah R. Ismail,[1,2] **Hamdy Kashtoh**,[1] **Mohamed A. Betiha**,[2] **Salem A. Abu Amr**,[3] **Kwang-Hyun Baek**,[1] **and Nour Sh. El-Gendy**[2,4]

[1]*Department of Biotechnology, Yeungnam University, Gyeongsan, Gyeongbuk 38541, Republic of Korea*
[2]*Egyptian Petroleum Research Institute (EPRI), PO 11727, NasrCity, Cairo, Egypt*
[3]*Health Safety and Environmental Management, International College of Engineering and Management, 111 Seeb, PO 2511, Muscat, Oman*
[4]*Center of Excellence, October University for Modern Sciences and Arts (MSA), 6th of October City, PO 12566, Giza, Egypt*

Correspondence should be addressed to Kwang-Hyun Baek; khbaek@ynu.ac.kr and Nour Sh. El-Gendy; nourepri@yahoo.com

Received 2 June 2022; Revised 16 July 2022; Accepted 15 September 2022; Published 2 November 2022

Academic Editor: Pratima Meshram

In this study, evaporation-induced self-assembly was applied to prepare amine-functionalized nano-silica (NH_2-Pr-SBA-15). That was simply used to immobilize *Bacillus stratosphericus* PSP8 lipase (E–NH_2–Pr-SBA-15), producing a nanobiocatalyst with good stability under vigorous shaking and a maximum lipase activity of 45 ± 2 U/mL. High-resolution *X*-ray diffractometer, Fourier transform infrared spectroscopy, N_2 adsorption-desorption, field-emission scanning electron, and high-resolution transmission electron microscopic analyses proved the successful SBA-15 functionalization and enzyme immobilization. Response surface methodology based on a 1/2 fraction-three-levels face center composite design was applied to optimize the biodiesel transesterification process. This expressed efficient percentage conversion (97.85%) and biodiesel yield (97.01%) under relatively mild operating conditions: 3.12 : 1 methanol to oil ratio, 3.08 wt.% E–NH_2–Pr-SBA-15 loading, 48.6°C, 3.19 h at a mixing rate of 495.53 rpm. E–NH_2–Pr-SBA-15 proved to have a long lifetime, operational stability, and reusability.

1. Introduction

The increased global population with the highly eminent use of transportation fuels and industrial activities dramatically intensifies greenhouse gas emissions, global warming, and the negative consequences of climate change [1, 2]. Consequently, there is a worldwide conduit towards sustainable and green fuels [3], i.e., biodiesel [4], bioethanol [5], biojet [6], and biogas [7], which play a vital role in achieving the three pillars of sustainable development:economy, society, and environment [3].

Nowadays, there is a tremendous worldwide investment in the long-chain fatty acid monoalkyl ester, i.e., biodiesel, which is a natural, eco-friendly, biodegradable, and sustainable alternative fuel to the nonrenewable petro-diesel without the need for any engine modifications [8]. However, the first-generation biodiesel from edible feedstock induced many environmental and societal concerns, negatively impacting food security and land use [2, 9]. Besides, the main bottlenecks in the biodiesel industry are the high cost of feedstock [4, 10], the massive consumption of nonsustainable homogenous catalysts in the transesterification process, and water in the washing step [11]. In addition to the possible decrease in biodiesel yield that may occur with the conceivable manifestation of saponification and the miscibility of the unreacted catalyst, which hurdles the glycerol recovery [12].

The valorization of sustainable resources such as waste cooking oil (WCO) into biodiesel is estimated to decrease the total cost of the transesterification process by two to three folds [10, 13, 14] and solve the environmental problems caused by the uncontrolled disposal of WCO [1, 15]. Nevertheless, the use of nano-bio-composite heterogeneous catalysts for biodiesel production in the form of nano-immobilized sustainable lipase enzyme has various advantages compared to conventional catalysts, including mild operating conditions and reasonable economics, ease of product separation and recovery, absence of side reactions, and the elimination of washing steps [16–19]. However, the efficiency, reusability, and catalytic stability of the nano-immobilized sustainable lipase and its tolerance to toxic short-chain alcohols are the main apprehensions for its application in the biodiesel industry [20, 21]. Therefore, finding new ways to avoid these negatives is one of the most critical challenges, and there are many suggested published methods for lipase immobilization to sustain its catalytic activity and enhance its stability, involving entrapment, encapsulation, cross-linking, covalent bonding, and physical adsorption [22–27].

The mesoporous silica, with its unique features of large surface area and tunable pores, is reported to be one of the most crucial immobilizing matrices for enzymes, enabling the excellent dispersion of active phase (enzymes or active metals) and biocatalyst-enhanced activity, high selectivity, and stability [28–30]. *Candida Antarctica* lipase immobilized on SBA-15 [31], and different functionalized mesoporous SBA-15 [32] have been reported for producing biodiesel from the nonedible *Calophyllum inophyllum* oil. Metal-impregnated SBA-15 has also been used for lipase immobilization for biodiesel production; for example, *Pseudomonas fluorescens* lipase immobilized over Ca-modified mesoporous SBA-15 [33]. Moreover, *Mucor miehei* and *Rhizopus oryzae* lipases [34], *Mucor miehei* lipase [35], *Candida rugosa* lipase [21], and *Burkholderia cepacia* lipase 1 [36] immobilized on SBA-15 have also been reported for biodiesel production. Besides, other organic functionalized SBA-15, for example, *Rhizomucor miehei* lipase immobilized on aldehyde-functionalized SBA-15 [37], *Candida antarctica*, *Thermomyces lanuginosus*, and *Rhizomucor miehei* lipases covalently immobilized on 3-glycidyloxypropyl trimethoxysilane modified mesoporous SBA-15 [38], *Actinomadura sediminis* lipase immobilized on oleic acid modified mesoporous SBA-15 [20], and porcine pancreatic lipase immobilized on mesoporous SBA-15/chitosan-glutaraldehyde matrix [39]. Amine-modified silica, either by post or direct modification, is one of the most important modified silica types because of the ease of enzyme immobilization via chemical and/or physical bonds, compared to thiol, carboxyl, or other organic modified silica, and the enhanced activity and stability [32, 40].

This manuscript aimed to prepare amine-functionalized nano-silica (NH_2-Pr-SBA-15) for the practical immobilization of *Bacillus stratosphericus* PSP8 lipase (E–NH_2–Pr-SBA-15) to ingeniously valorize sustainable WCO into biodiesel. Response surface methodology (RSM) based on the 1/2 fraction-three-level face-centered central composite design (FCCCD) of experiments was applied for statistical optimization of the transesterification process to maximize biodiesel yield. Furthermore, the reusability of the E–NH_2–Pr-SBA-15 for successive transesterification processes has been done to prove its stability. Physicochemical characterization of the produced biodiesel (B100) has also been performed to assure the feasibility of the prepared nano E–NH_2–Pr-SBA-15 in the biodiesel industry.

2. Materials and Methods

2.1. Materials. Bacillus stratosphericus PSP8 lipase was produced in a ten-liter self-sterilizer bioreactor (Biotron Life SL, Korean Republic) as previously reported by Ismail et al. [18]. Methanol (AR grade) and absolute alcohol (≥99.5%) were obtained from E. Merck KG Co. (Darmstadt, Germany). Tetraethyl orthosilicate (TEOS), 3-aminopropyltriethoxysilane, Poly(ethylene glycol)-block-poly(propylene glycol)-block-poly(ethylene glycol), diacrylate (PEG-PPG-PEG, i.e., Pluronic-P123), and hexamethyldisilazane were bought from Sigma-Aldrich Chemie GmbH (Taufkirchen, Germany). WCO with 35.68% saturated fatty acids, 30.47% palmitic (C16 : 0) and 5.21% stearic (C18 : 0), and 64.32% unsaturated fatty acids, 24.79% oleic (C18 : 1), 39.03% linoleic (C18 : 2), and 0.503% linolenic (C18 : 3), was collected as domestic waste and filtered to remove any unwanted food debris. Such WCO was characterized by relatively high density (0.9271 g/cm^3), viscosity (48.7 cSt), total acid number of 2.85 mg KOH/g oil, water content (480.6 ppm), iodine value (121 mg I_2/100 g oil), and saponification value (191 mg KOH/g oil). To decrease the pre-esterification process's energy, catalyst, and time consumption, the filtered WCO was used as it is without any pretreatment for water removal or decreasing the TAN content. Besides, water in WCO is essential for lipase-enhanced enactment since the water film around the enzyme stabilizes and retains its activity [18, 19, 32].

2.2. Preparation of Amine-Functionalized Nano-Silica (NH_2-Pr-SBA-15). The evaporation-induced self-assembly (EISA) method was applied to prepare NH_2-Pr-SBA-15, according to Zhu et al. [41]. In a 300 mL Teflon beaker and at room temperature, 6 g of Pluronic - P123 was dissolved in a mixture of 0.1 N HCl, 150 mL anhydrous ethanol, and 4 mL mesitylene. After complete dissolution and under gentle stirring, a mixture of 4 : 1 (v/v) tetraethoxysilane (TEOS) and 3-aminopropyltriethoxysilane (APTES, $NH_2(CH_2)_3Si(OC_2H_5)_3$) was drop-wisely added. Then, the temperature was elevated to 45 °C for 30 min to initiate the hydrolysis of the silica precursor (i.e., the TEOS). After that, the mixture was poured on a Teflon Petri dish and left for two days. The obtained powder was neutralized with 0.05 N NaOH to remove HCl and break the NH_3-Cl bond. Then, the powder was redispersed in a mixture of hexamethyldisilazane and ethanol (4.5 mL:20 mL) and retained in an ultrasonic for 15 min at room temperature to complete the removal of excess P123 and unreacted silica precursor. Finally, the free-surfactant NH_2-Pr-SBA-15 was washed with ethanol for five cycles and then vacuum dried overnight at 40°C.

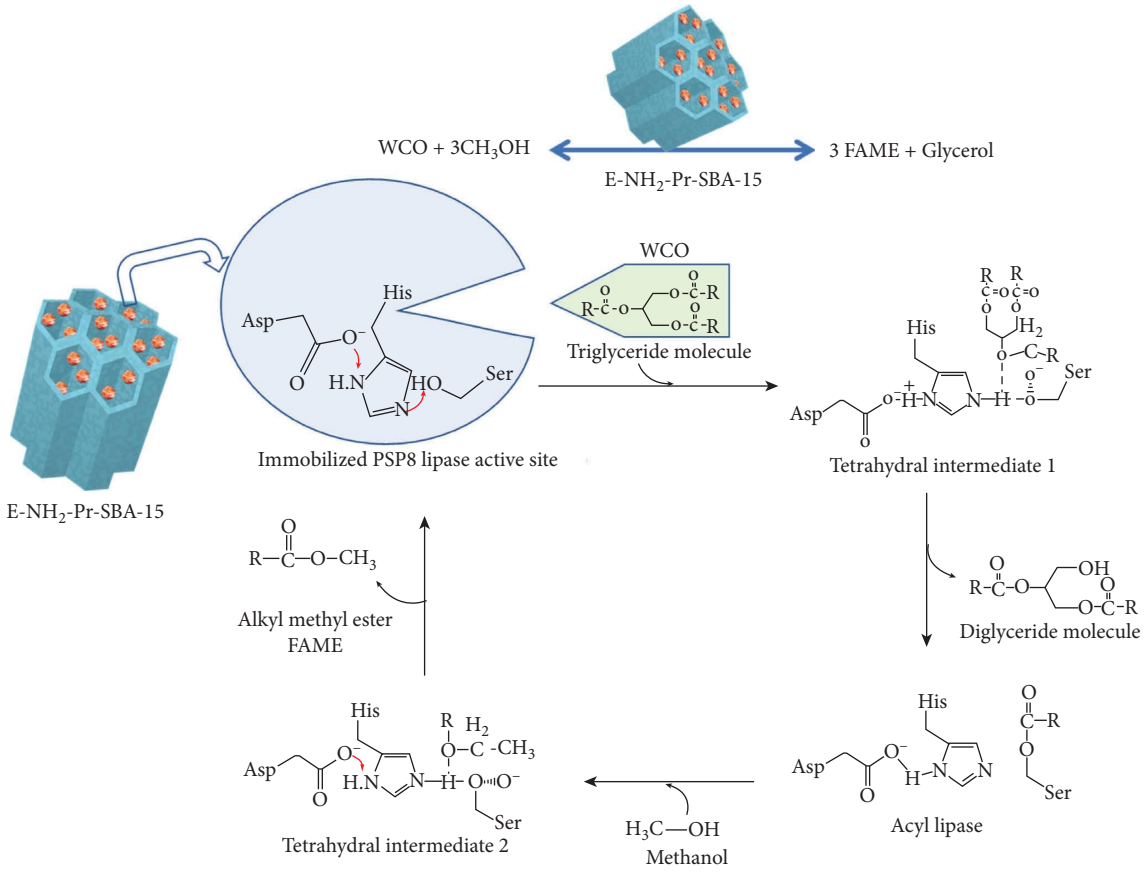

Scheme 1: The transesterification mechanism by the immobilized PSP8 lipase E–NH_2–Pr-SBA-15.

2.3. Lipase Immobilization. In a 100 mL water/ethanol mixture (80 : 20 v/v), a prescribed amount of lyophilized PSP8 lipase was added to 1 g of the pre-dispersed NH_2-Pr-SBA-15 in a final concentration range of 0.01–1.5% w/w. Then, it was blended for six *h* after the adjustment of the pH to pH7 using 0.05 M phosphate buffer. Finally, the immobilized lipase was separated by centrifugation. Figure 1 briefly illustrates the steps of lipase immobilization.

The best lipase loading was demarcated by assessing the immobilized lipase activity according to the technique reported by Castro-Ochoa et al. [42] using p-nitrophenyl-laurate (*p*NPL) as a substrate. A previously prepared standard curve using 10–1000 U/mL of Amano lipase A from *Aspergillus Niger* (Sigma Aldrich, Darmstadt, Germany) has been used. One unit (U) of lipolytic activity was defined as the amount of lipase that released 1 mol of *p*-nitrophenol (molar absorption coefficient 4.6 $mM^{-1}\,cm^{-1}$) from pNPL within 30 min under the tested conditions.

The enzyme leaching test of the immobilized lipase amine-functionalized mesoporous SBA-15 was performed according to the technique described by Gao et al. [43] using the preselected optimum enzyme loading ratio. The immobilized lipase was suspended in 0.05 M phosphate buffer at pH7 at a final concentration of 1.25 mg/mL and shaken at 200 rpm. At different prescribed time intervals, aliquots of the suspensions were withdrawn, centrifuged, and the residual lipase activities were determined as reported by Castro-Ochoa et al. [42].

A preliminary investigation of the capabilities of the SBA-15, NH_2-Pr-SBA-15, and immobilized lipase at a preselected optimum loading ratio for biodiesel production has been performed under the following operating conditions:6 : 1 methanol:oil (M : O molar ratio), six wt.% nanobiocatalyst loading, 60°C, three *h*, and 400 rpm.

2.4. Catalyst Characterization. The prepared SBA-15, NH_2-Pr-SBA-15, and the nano-immobilized enzyme with the preselected optimum enzyme loading ratio E–NH_2–Pr-SBA-15 were characterized for their crystalline structure using a high-resolution X-ray diffractometer (XRD; PANalytical XPERT PRO MPD, EA Almelo, the Netherlands) coupled with Cu kα radiation source ($\lambda = 1.5418$ Å). Moreover, the functional species of the prepared nanobiocatalyst were identified via Fourier transform infrared spectroscopy (FTIR; Perkin Elmer Spectrum One, Shelton, CT, USA). Their specific surface areas were determined by the Brunauer-Emmett-Teller (BET) technique using a low-temperature N_2 adsorption-desorption isotherm (NOVA3200e, Quantachrome, FL, USA). The catalyst sample was tested for pore diameter, volume, and size distribution by applying the Barret-Joyner-Halenda (BJH) method. The morphology and

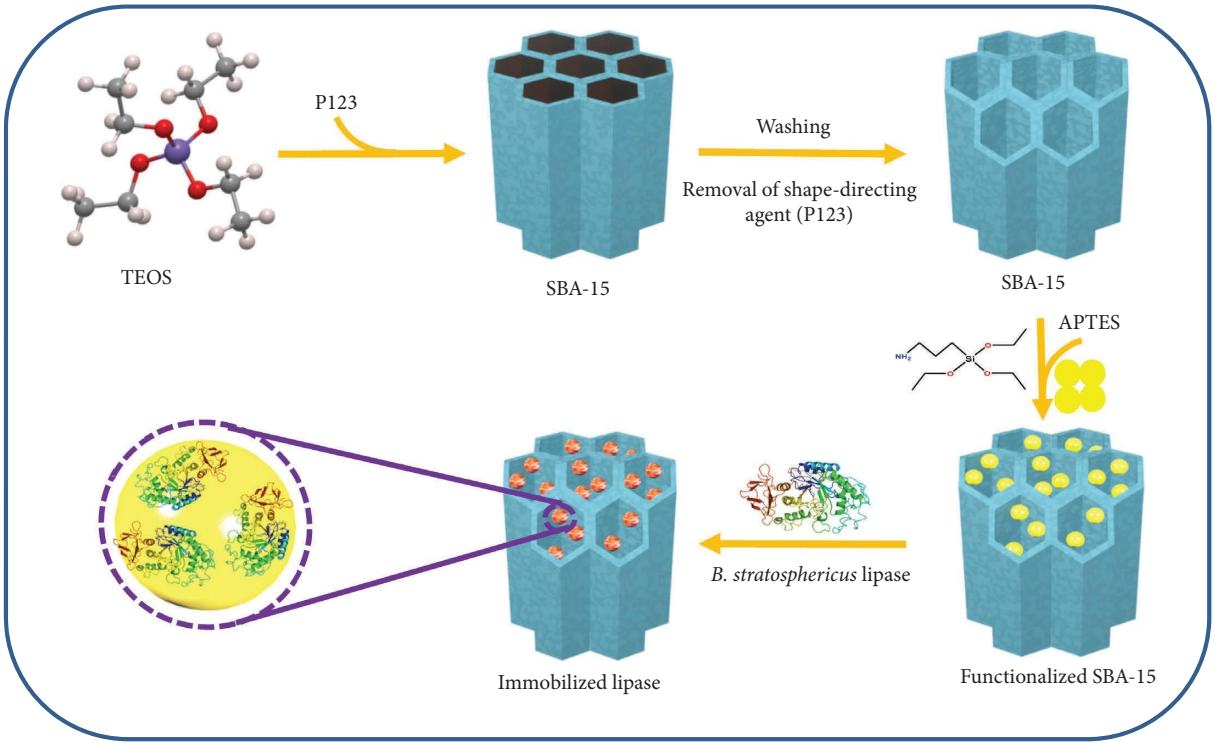

Figure 1: Steps for *Bacillus stratosphericus* lipase immobilization on the prepared NH_2-Pr-SBA-15.

structure of the as-prepared catalysts were determined by the field-emission scanning electron microscope (FE-SEM S-4800, Hitachi High-Technologies Corporation, Tokyo, Japan) and high-resolution transmission electron microscope (HR-TEM, JEOL-JEM 2100F, 80–200 kV, Tokyo, Japan).

2.5. Statistical Optimization of the Biodiesel Transesterification Process. Response surface methodology (RSM) is based on a 1/2 fraction-three-levels face center composite design (FCCD) of five experimental factors; M : O (molar ratio, A), nano-immobilized enzyme concentration (wt.%, B), reaction temperature (°C, C), reaction time (h, D), and mixing rate (rpm, E) were employed. A design of 32 batch processes with 16 factorial, ten axial, and six central points was implemented to avoid bias (Table 1). The transesterification batch process was performed according to Ismail et al. [18] in an automized magnetically stirred three-necked 25 mL reactor equipped with a thermometer and a reflux condenser set at the prescribed reaction temperature, time, and stirring speed. The prescribed concentration of immobilized enzyme was added after the M : O mixture reached the prerequisite reaction temperature. Then the reaction mixture, at the end of each batch, was allowed to separate overnight. Next, pure glycerol and nanobiocatalyst were obtained by centrifugation of the separated lower layer at 10,000 rpm for 10 min. Finally, a rotary evaporator set at 65°C and 20 kPa was used to recycle the excess unreacted methanol for reusability. Then, the obtained purified biodiesel was applied for further physicochemical characterization according to the standard test methods for petroleum products of the American Society for Testing and Materials [44].

The design Expert 6.0.7 software (Stat-Ease Inc., Minneapolis, USA) was used to design the transesterification experiments and inspect the interactive effects of the different physicochemical parameters on the valorization of WCO into biodiesel using the immobilized lipase. It was also applied to statistically optimize the transesterification process for maximizing the biodiesel yield, performing the regression and graphical analyses of the obtained data and the statistical analysis of variance (ANOVA) of the predicted regression model equation, estimating the response surface.

The valorization of WCO into biodiesel was calculated according to Ismail et al. [18] via the depletion of the kinematic viscosity of the oil layer, at 40°C using the following equation:

$$\text{conversion}\,(\%) = \left(1 - \frac{V_{BD}}{V_{WCO}}\right) \times 100, \quad (1)$$

where V_{BD} and V_{WCO} are the viscosity of the produced biodiesel and valorized WCO, respectively. All measurements were in triplicates and the average data were calculated within a standard deviation (StD) range of ±2%, and $P < 0.05$ is statistically significant at $\alpha = 0.05$ level, 95% confidence interval.

The produced fatty acid methyl esters (FAME, Figure 2) were identified by gas chromatography equipped with a flame ionization detector (GC/FID model HP Agilent 7890, CA, USA) using a prepared reference mixture of palmitate, stearate, oleate, linoleate, and linolenate (Sigma–Aldrich

Table 1: Design of experiments for the transesterification process using E–NH_2–Pr-SBA-15 with the experimental and predicted response values.

No.	A	B	C	D	E	% conversion		Biodiesel yield wt.%	
	M : O molar ratio	Immobilized enzyme wt.%	Temperature °C	Time *h*	Mixing rate rpm	Actual	Predicted	Actual	Predicted
1	4.50	6.00	50.00	3.00	450.00	62.1	64.04	68.3	68.84
2	4.50	6.00	50.00	2.00	450.00	35.1	32.86	39.5	36.89
3	6.00	9.00	60.00	2.00	300.00	57.3	57.29	60.8	60.71
4	3.00	9.00	60.00	2.00	600.00	77.6	77.39	83.4	83.21
5	4.50	6.00	50.00	3.00	450.00	63.4	64.04	68.2	68.84
6	3.00	3.00	60.00	2.00	300.00	34.1	34.56	42.4	42.76
7	6.00	3.00	60.00	2.00	600.00	38.1	38.27	43.2	43.92
8	4.50	6.00	50.00	3.00	600.00	61.2	61.75	68.1	67.08
9	3.00	9.00	40.00	2.00	300.00	63.8	64.19	69.7	69.63
10	3.00	3.00	40.00	2.00	600.00	33.9	34.46	38.8	39.54
11	6.00	6.00	50.00	3.00	450.00	79.2	78.95	84.0	82.60
12	4.50	3.00	50.00	3.00	450.00	78.9	76.78	83.8	80.58
13	4.50	6.00	50.00	3.00	450.00	62.3	64.04	68.0	68.84
14	4.50	6.00	50.00	3.00	450.00	62.4	64.04	68.3	68.84
15	6.00	9.00	40.00	4.00	300.00	58.5	58.39	63.4	63.03
16	4.50	6.00	50.00	3.00	450.00	64.4	64.04	68.2	68.84
17	4.50	9.00	50.00	3.00	450.00	90.7	91.96	93.4	95.64
18	4.50	6.00	50.00	4.00	450.00	39.7	41.08	43.5	45.13
19	6.00	9.00	60.00	4.00	600.00	46.8	46.10	52.8	52.31
20	6.00	3.00	40.00	2.00	300.00	40.1	40.86	43.1	43.94
21	6.00	9.00	40.00	2.00	600.00	83.4	83.50	87.1	87.39
22	4.50	6.00	50.00	3.00	300.00	57.3	55.90	61.3	61.34
23	3.00	3.00	40.00	4.00	300.00	74.0	74.36	80.0	80.08
24	4.50	6.00	60.00	3.00	450.00	46.7	47.66	54.5	54.99
25	4.50	6.00	40.00	3.00	450.00	58.2	56.38	64.5	63.03
26	6.00	3.00	60.00	4.00	300.00	36.7	36.66	41.3	41.36
27	3.00	6.00	50.00	3.00	450.00	85.4	84.80	89.0	89.42
28	3.00	9.00	60.00	4.00	300.00	74.1	73.69	80.4	79.55
29	6.00	3.00	40.00	4.00	600.00	78.9	78.97	83.7	84.14
30	4.50	6.00	50.00	3.00	450.00	66.2	64.04	68.1	68.84
31	3.00	3.00	60.00	4.00	600.00	64.8	64.56	68.1	68.07
32	3.00	9.00	40.00	4.00	600.00	63.9	63.59	68.9	68.43

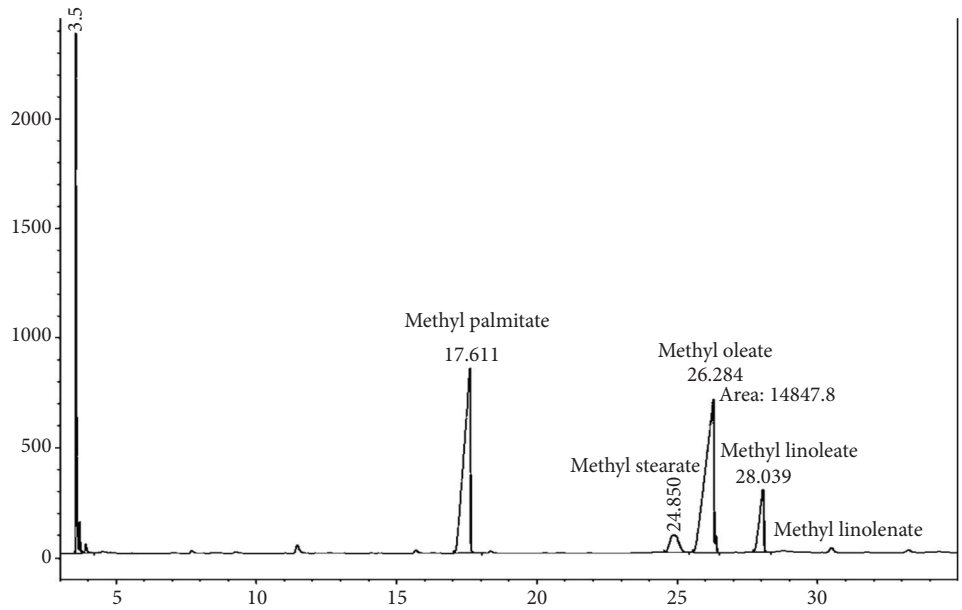

Figure 2: FAME profile of the produced biodiesel.

Chemie GmbH, Taufkirchen, Germany), and linolenate was injected as an internal standard [18]. Then, the biodiesel yield was calculated according to Nassar et al. [2] based on the calculated % purity as follows:

$$\%\text{Purity} = \text{PAR} \times \left(\frac{\text{weight of internal standard}}{\text{Weight of biodiesel}}\right) \times 100, \quad (2)$$

where PAR is the ratio of the total FAME peak area to that of the added internal standard.

$$\text{Biodieselyield}\% = \%\text{purity} \times \left(\frac{\text{weight of biodiesel}}{\text{weight of WCO}}\right). \quad (3)$$

2.6. Reusability of the Prepared Nano-Immobilized PSP8 Lipase. That was done according to Karimi (2016) to evaluate the stability of the prepared nano-immobilized lipase [23]. The transesterification reaction of WCO was performed at the predicted optimum conditions. The nanobiocatalyst was separated from the reaction mixtures at the end of each batch by centrifugation at 10,000 rpm for 10 min, then washed with phosphate buffer (0.2 M, pH7) and tert-butanol (1 : 1 v:v), and finally lyophilized by a bench-top freeze dryer (Eyela-FDU-1200, Bohemia, NY, USA). The recovered nanobiocatalyst was then reused in a subsequent transesterification reaction at the optimum conditions. Finally, the reusability of immobilized lipase was inspected by repeating the aforementioned steps for eight successive cycles, and the % conversion and biodiesel yield were determined for each transesterification cycle.

2.7. Statistical Analysis. Statistical analysis for the obtained data was performed using SPSS version 26 (Informer Technologies, Inc., Los Angeles, CA, USA). Tukey was used to evaluate the significant differences between the obtained based on a significant interval of 95% ($p = < 0.05$).

3. Results and Discussion

3.1. Effect of Lipase Loading. The prepared nanobiocatalyst (E–NH_2–Pr-SBA-15) with a loading ratio of 1% (Figure 3(a)) expressed the maximum lipase activity, recording 45 ± 2 U/mL ($p < 0.0001$ at $\alpha = 0.05$ level, 95% confidence interval). However, any further increment in lipase loading (Figure 3(a)) did not show any elevation in lipase activity ($0.153 \leq p \leq 0.895$ at $\alpha = 0.05$ level, 95% confidence interval). The 1% loading was selected for further experiments to avoid the possible occurrence of retardation in the substrate and product diffusion. According to Li et al. [26], a relatively high enzyme loading ratio would cause intermolecular steric hindrance. As calculated by the method reported by Sun et al. [45], the specific enzyme activity reached approximately 44,550 U/g. That was higher than that reported for immobilized *Candida Antarctica* lipase onto amine SBA-15, which recorded 12,000 U/g [32].

3.2. The Stability of the Prepared E–NH_2–Pr-SBA-15 under Shaking Conditions. There was a continuous activity loss with time, under vigorous shaking at 200 rpm (Figure 3(b)). However, the prepared nanobiocatalyst (E–NH_2–Pr-SBA-15) expressed reasonable stability, as it retained approximately $77.14 \pm 1.4\%$ of its initial activity after 120 h ($p < 0.0001$ at $\alpha = 0.05$ level, 95% confidence interval). That was much better than those reported by Gao et al. [22], where the immobilized *Candida* sp. 99–125 lipase onto mesoporous silica via adsorption and cross-linking retained only up to 9.6% and 60% of its initial activity after 120 h under shaking at 200 rpm, respectively. It is also worth mentioning that approximately $67.70 \pm 1.4\%$ and $56.92 \pm 1.4\%$ of the immobilized PSP8 lipase initial activity was retained after 7 and 10 d, respectively ($p < 0.0001$ at $\alpha = 0.05$ level, 95% confidence interval). Consequently, it would indicate that the prepared NH_2-Pr-SBA-15 effectively prevented the leaching off of the immobilized lipase. Thus, this recommends the application of the prepared E–NH_2–Pr-SBA-15 in the industrial transesterification process, as it usually takes place under vigorous shaking conditions to overcome the mass transfer limitations.

3.3. The Primary Transesterification Activity of the Prepared Nanocatalysts. The preliminary investigation for the transesterification capabilities of the prepared catalysts, proved biodiesel yields of approximately 6%, 32%, and 67% (±1.5%) using SBA-15, NH_2-Pr-SBA-15, and E–NH_2–Pr-SBA-15, respectively ($p < 0.0001$ at $\alpha = 0.05$ level, 95% confidence interval). That indicated the efficient transesterification activity of the immobilized lipase.

3.4. Catalyst Characterization. The XRD patterns of the prepared catalysts are illustrated in Figure 4(a) and prove their crystallinity. Besides, the prominent peak at (100) and the lower intensity peaks that appeared at (110) and (200) are typical for the ordered mesoporous SBA-15 with hexagonal arrays and p6mm symmetry [46]. Moreover, the NH_2-Pr-SBA-15 nearly retained the same pattern as the unfunctionalized SBA-15, proving that grafting by APTES did not affect its structural integrity. Disappeared peaks at (110 and 200) with the decreased intensity at (100) in the E–NH_2–Pr-SBA-15 XRD pattern (Figure 4(a)) might be attributed to the presence of organic moieties. Consequently, it would confirm the successful immobilization of PSP8 lipase onto the prepared NH_2-Pr-SBA-15. A similar observation was reported by Veisi et al. [47] and attributed to the possible disorderliness occurring by the direct functionalization of SBA-15, which might cause partial shielding of the tiny pores and/or the presence of organic moieties, which might affect the scattering angle within the unit cell.

The FTIR spectra of SBA-15, NH_2-Pr-SBA-15, and E–NH_2–Pr-SBA-15 are illustrated in Figure 4(b). The SBA-15 showed FTIR peaks at 1075 and 800 cm^{-1} of the–Si–O asymmetric and symmetric stretching vibration, respectively, a peak around 458 cm^{-1} of the bending vibration of Si–O–Si group and a peak around 945 cm^{-1} of Si–OH

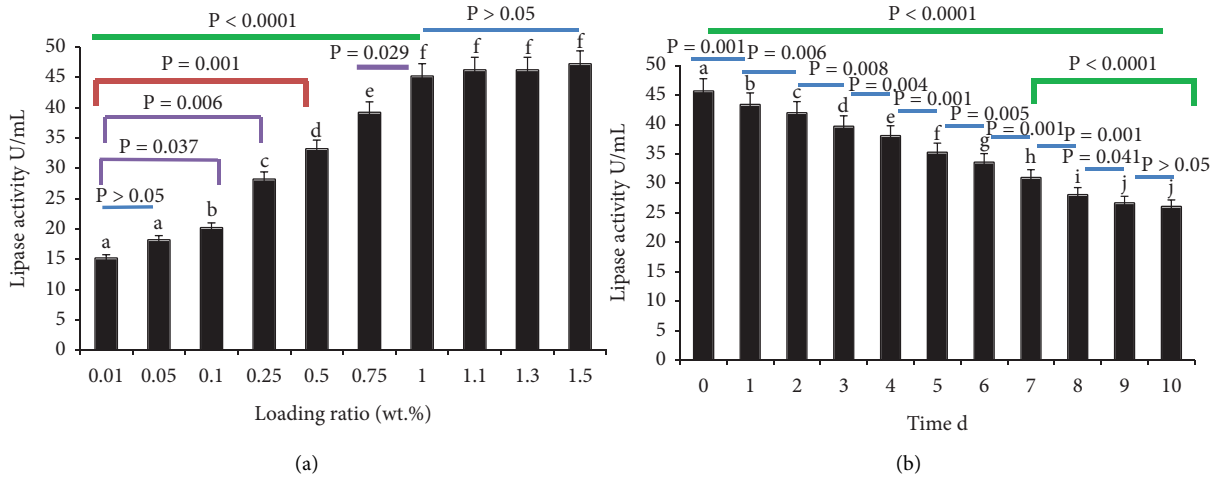

Figure 3: Effects of lipase loading (a) and vigorous shaking (b) on the prepared nanobiocatalyst E–NH_2–Pr-SBA-15 activity and stability.

bending vibration [46]. Besides, the broad peak appeared around 3452 cm^{-1}, which might be attributed to the terminated hydroxyl groups, in addition to the band of–OH deformation vibration around 1630 cm^{-1} [48]. The functionalized NH_2-Pr-SBA-15 nanoparticles displayed additional peaks at 2928 and 2856 cm^{-1} that could be assigned to C–H's asymmetric and symmetric stretching vibration in the 3-aminopropyltriethoxysilane, and the weak band at 3290 cm^{-1} might be ascribed to–NH_2 group [49]. The disappearance of the Si–OH bending vibration band around 945 cm^{-1} might indicate the involvement of Si–OH in the functionalization reaction [46]. Moreover, the FTIR peak around 1229 cm^{-1} is due to Si–C bond. The weak FTIR peaks around 1540 and 1400 cm^{-1} are attributed to the asymmetric and symmetric vibrations of–NH_2, confirming the successful preparation of NH_2-Pr-SBA-15 nanoparticles. Comparing the spectrum of NH_2-Pr-SBA-15 to that of E- NH_2-Pr-SBA-15 nanobiocomposite, the increase in the intensities of the peaks around 2930 and 600 cm^{-1} might be attributed to the C–H and N–H stretching vibrations of the lipase enzyme [46]. Besides, the appearance of peaks within 1780 to 1860 cm^{-1} would be attributed to the *C=O* of peptide and carboxylic moieties in the lipase enzyme [50]. The increase in intensities of peaks around 1440 and 1530 cm^{-1} besides the appearance of the peak around 1640 cm^{-1} indicates–CH and–NH_2 moieties of the lipase enzyme [21]. Furthermore, the sharp decrease in intensity of peak at 3450 cm^{-1} gave another indication of electrostatic interaction between the lipase enzyme and –OH of the silica [46].

The FTIR analysis would prove the involvement of the surface functional groups of SBA-15 and the functionalized NH_2-Pr-SBA-15 into the lipase immobilization via covalent bonding, not only via the conventional hydrophobic and/or electrostatic interactions. According to Salvi and Yadav [51]; the observed high stability and activity of the immobilized PSP8 lipase onto the NH_2-Pr-SBA-15 might be attributed to the immobilization via covalent bonding that provides efficient strengthened immobilized constancy between the lipase molecules and the immobilizing supporting material and consequently reduces the enzyme leakage.

It can be depicted from the N_2-physisorption analysis illustrated in Figure 4(c) That all isotherms of the prepared SBA-15, NH_2-Pr-SBA-15, and E–NH_2–Pr-SBA-15 exhibited type IV with H1-hysteresis loops and indicated according to Betiha et al. [52] the presence of mesopores. The materials showed a steep increase in N_2-adsorption (capillary condensation step) at P/P_0 of 0.57–0.85, suggesting high uniform mesoporous materials according to Gao et al. [22]. Upon functionalization, the capillary condensation shifted to lower P/P_0, confirming shrinkage in pore diameter due to the presence of pendant organic moieties (–Si-$CH_2CH_2CH_2$–NH_2), that further decreased upon the enzyme immobilization. The desorption hysteresis loop likely became broader after enzyme immobilization, which might be attributed, according to Pinto et al. [36]; to the presence of protein inside the pores, causing a delay in the nitrogen desorption. After introducing–Si-$CH_2CH_2CH_2$–NH_2 and enzyme, the specific surface area decreased from 802 m^2/g for virgin SBA-15 to 612 and 579 m^2/g, respectively. That trend was consistent with decreasing pore volume and pore size, recording 1.02 cc/g and 3.55 nm for SBA-15, 0.911 cc/g, and 2.9 nm for NH2-Pr-SBA-15 0.89 cc/g and 2.81 nm for E–NH_2–Pr-SBA-15, respectively.

That recorded decrease in specific surface area, porevolume, and size confirmed, according to Salvi and Yadav [51]; the successful functionalization and enzyme immobilization. A similar observation was reported by Kou et al. [46] for SBA-15 functionalization by N(-2-aminoethyl)-3-aminopropyl and 3-aminopropyl groups followed by lactase enzyme immobilization. Moreover, according to Badiei et al. [53] that would also indicate the occurrence of modification within the inner surface of the silica wall. Besides the homogenous distribution of the immobilized enzyme onto the SBA-15 surface and within its pores [36]. Not only that, but according to Kou et al. [46] those results would also indicate entrapment of the enzyme molecules within the silica channels besides its surface adsorption onto the mesoporous

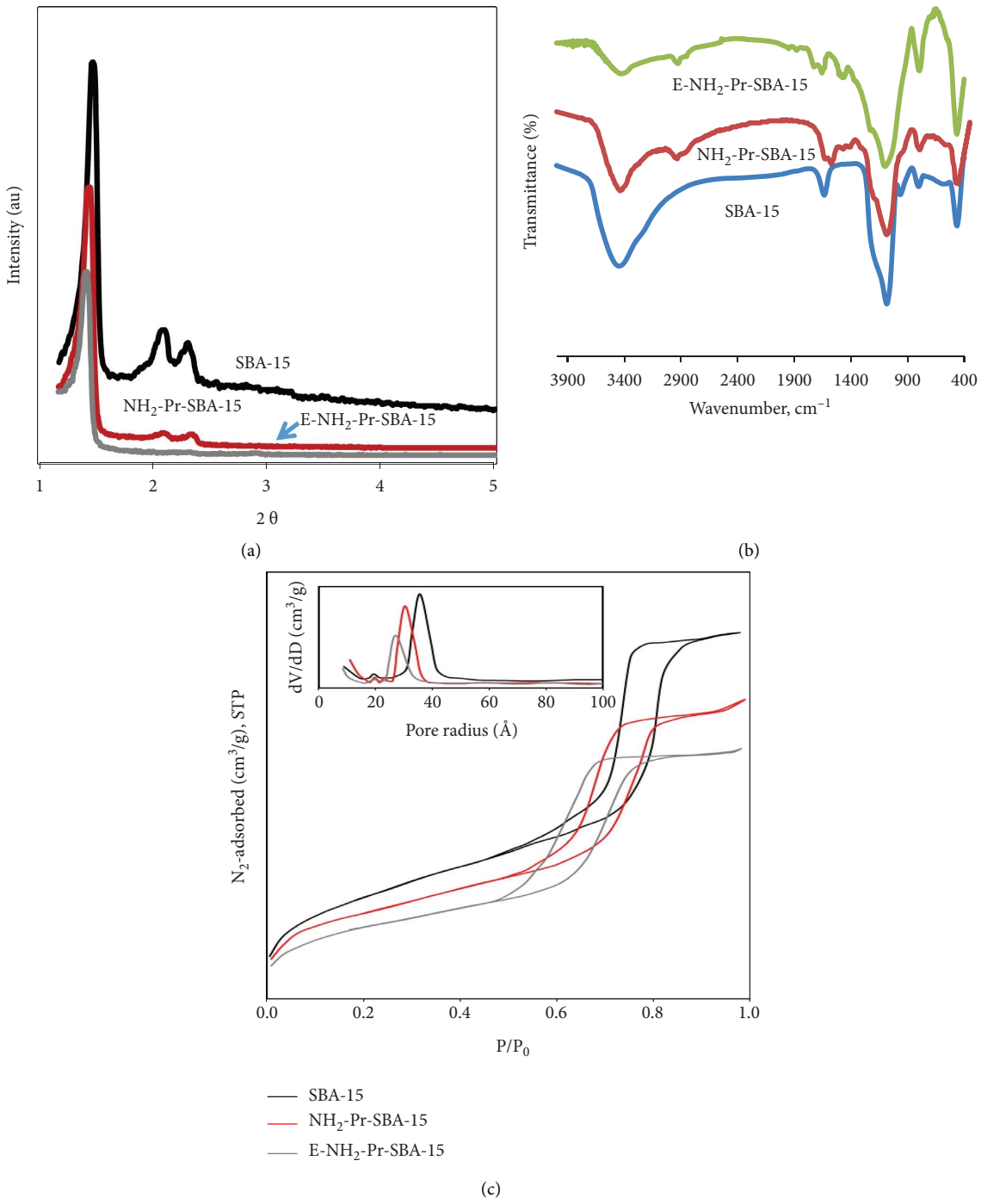

Figure 4: The XRD (a), FTIR (b), and N_2 adsorption/desorption isotherms and pore diameter distribution (c) of the prepared catalysts.

structure. Consequently, those obtained results would explain the relatively high stability of the immobilized enzyme under vigorous shaking.

The FESEM images (Figures 5(a)–5(c)) show aggregates of rope-like nanoparticles that kept their uniform structure after amine-functionalization and lipase immobilization. The immobilized lipase is well adsorbed onto the NH_2-Pr-SBA-15 nanoparticles (Figure 5(c)). The SBA-15 HRTEM image (Figure 5(d)) showed the existence of regular ordered mesoporous channels in the form of a honeycomb-type network. The HRTEM image of the NH_2-Pr-SBA-15 (Figure 5(e)) confirmed the XRD-analysis as mentioned above and showed more observable arrangements of conservative mesoporous channels. This, according to Kou et al. [46]; might indicate the intact SBA-15 Si–O–Si network and proves that SBA-15 pores did not collapse or break down during the functionalization reaction. However, these pores appeared embedded with organic moieties in the

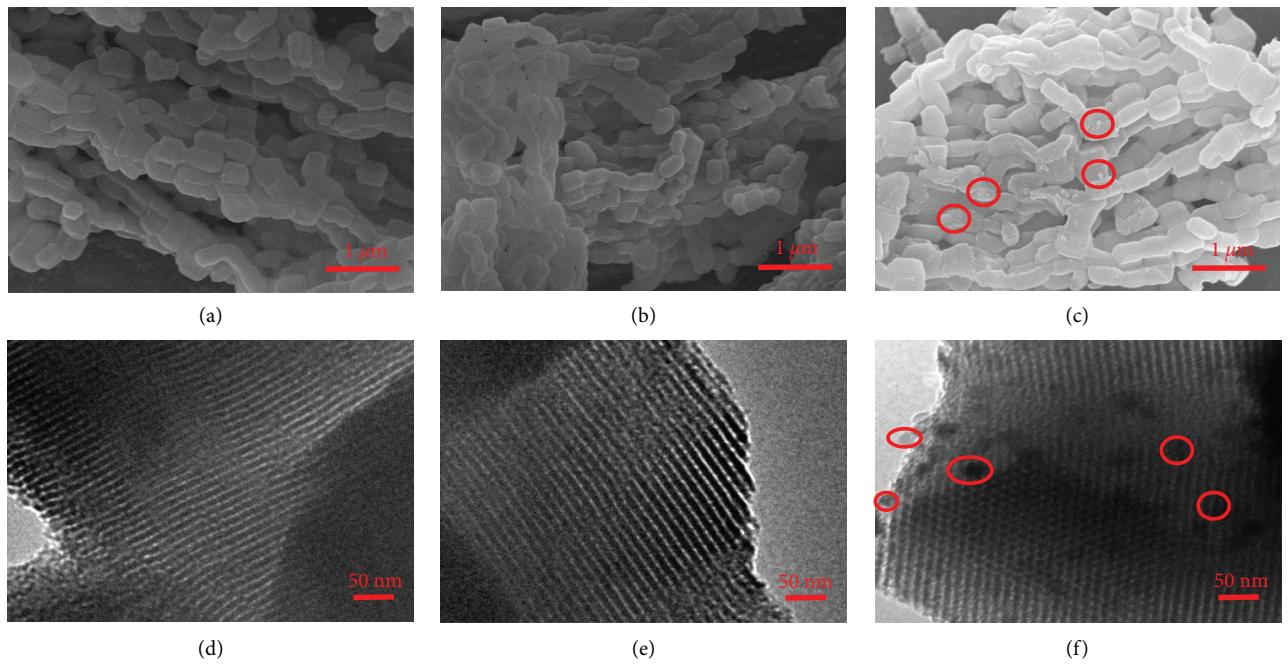

Figure 5: The FESEM images of SBA-15 (a), NH_2-Pr-SBA-15 (b), and E–NH_2–Pr-SBA-15 (c) and HRTEM images of SBA-15 (d), NH_2-Pr-SBA-15, (e) and –NH_2–Pr-SBA-15 (f).

E–NH_2–Pr-SBA-15 image, and the pore wall was less specific than virgin the SBA-15, but the ordered structure was retained (Figure 5(f)).

3.5. Mathematical Representation of the Transesterification Process. Based on the obtained experimental results listed in Table 1, the transesterification process has been represented by two quadratic model equations; one was predicted for the % conversion (Y_1 eq.(4)), and the other was elucidated for the biodiesel yield (Y_2, eq. (5)). Then, the rationality of the two predicted model equations was validated by the F-test and the analysis of variance ANOVA, as represented in Table 2.

$$\begin{aligned} Y_1 = {} & 64.04 - 2.92A + 7.59B - 4.36C + 4.11D + 2.93E \\ & + 17.84A^2 + 20.34B^2 - 12.01C^2 - 27.06D^2 \\ & - 5.21E^2 - 1.28AB - 6.06AC - 4.09AD \\ & + 3.78AE + 2.46BC - 9.19BD - 0.80BE \\ & - 2.43CD + 0.087CE - 1.66DE, \end{aligned} \tag{4}$$

$$\begin{aligned} Y_2 = {} & 68.84 - 3.41A + 7.53B - 4.02C + 4.12D + 2.87E \\ & + 17.17A^2 + 19.27B^2 - 9.83C^2 - 27.83D^2 \\ & - 4.63E^2 - 1.27AB - 6.01AC - 3.15AD \\ & + 4.47AE + 2.43BC - 8.82BD - 0.57BE \\ & - 2.78CD + 0.019CE - 1.76DE. \end{aligned} \tag{5}$$

3.6. The Main and Interactive Effects of the Studied Factors on the Transesterification Process. The Pareto charts (Figure 7) showed that the reaction temperature expressed a more negative impact than the M : O molar ratio on the transesterification process, but the catalyst loading, reacting time, and mixing rate expressed a positive impact transesterification process. However, doubling the reaction time and mixing rate would decrease the transesterification efficiency. It is worth mentioning the sufficient tolerance of the prepared nanobiocatalyst E–NH_2–Pr-SBA-15 to the higher concentration of methanol, whereas the positive doubling effect of methanol M : O molar ratio on the transesterification efficiency was evident in the Pareto chart (Figure 7). The interaction effects of; catalyst concentration and reaction time > M : O and reaction temperature > catalyst concentration and reaction time > M : O and reaction time > reaction temperature and time > reaction time and mixing rate > M : O and catalyst concentration > catalyst concentration and mixing rate, expressed negative impact on the transesterification efficiency with a decreasing order. At the same time, the interaction between M : O and mixing rate > catalyst concentration and reaction temperature > reaction temperature and mixing rate expressed a positive impact on the transesterification efficiency with a decreasing order.

The curvatures of the five factors from the center point in the perturbation plots (Figure 7) confirmed the statistical data obtained from ANOVA (Table 2) and Pareto charts (Figure 7), i.e., the significant effect of each of the studied parameters. In comparison, all of the independent variables within the studied range expressed a very high statistically significant effect on the transesterification process ($p < 0.0001$) except for the higher mixing rate (E ∗ E), which expressed a negative statistically significant effect ($0.001 \le p \le 0.0022$). Moreover, the curvatures (Figure 7)

Table 2: Analysis of variance ANOVA for the predicted model equations.

Source	SS*	DF*	MS*	F-value	Prob > F	Remarks
Model eq. 4	8187.22	20	409.36	122.11	<0.0001	V. highly significant
A	153.71	1	153.71	45.85	<0.0001	V. highly significant
B	1036.64	1	1036.64	309.24	<0.0001	V. highly significant
C	342.35	1	342.35	102.12	<0.0001	V. highly significant
D	304.22	1	304.22	90.75	<0.0001	V. highly significant
E	154.29	1	154.29	46.03	<0.0001	V. highly significant
A^2	783.06	1	783.06	233.59	<0.0001	V. highly significant
B^2	1017.93	1	1017.93	303.65	<0.0001	V. highly significant
C^2	355.02	1	355.02	105.91	<0.0001	V. highly significant
D^2	1802.07	1	1802.07	537.57	<0.0001	V. highly significant
E^2	66.83	1	66.83	19.94	0.0010	Significant
AB	26.01	1	26.01	7.76	0.0177	Possibly significant
AC	588.06	1	588.06	175.42	<0.0001	V. highly significant
AD	267.32	1	267.32	79.74	<0.0001	V. highly significant
AE	228.01	1	228.01	68.02	<0.0001	V. highly significant
BC	97.02	1	97.02	28.94	0.0002	Highly significant
BD	1350.56	1	1350.56	402.88	<0.0001	V. highly significant
BE	10.24	1	10.24	3.05	0.1083	Nonsignificant
CD	94.09	1	94.09	28.07	0.0003	Highly significant
CE	0.12	1	0.12	0.037	0.8519	Nonsignificant
DE	44.22	1	44.22	13.19	0.0039	Significant
Residual	36.88	11	3.35			
Pure error	12.71	5	2.54			
Corrected total	8224.10	31				
Model eq. 5	7926.22	20	396.31	119.25	<0.0001	V. highly significant
A	208.76	1	208.76	62.82	<0.0001	V. highly significant
B	1020.01	1	1020.01	306.92	<0.0001	V. highly significant
C	290.40	1	290.40	87.38	<0.0001	V. highly significant
D	305.05	1	305.05	91.79	<0.0001	V. highly significant
E	148.49	1	148.49	44.68	<0.0001	V. highly significant
A^2	725.77	1	725.77	218.39	<0.0001	V. highly significant
B^2	914.12	1	914.12	275.06	<0.0001	V. highly significant
C^2	237.60	1	237.60	71.50	<0.0001	V. highly significant
D^2	1905.39	1	1905.39	573.33	<0.0001	V. highly significant
E^2	52.67	1	52.67	15.85	0.0022	Significant
AB	25.76	1	25.76	7.75	0.0178	Possibly significant
AC	577.20	1	577.20	173.68	<0.0001	V. highly significant
AD	196.70	1	196.70	59.19	<0.0001	V. highly significant
AE	319.52	1	319.52	96.14	<0.0001	V. highly significant
BC	94.58	1	94.58	28.46	0.0002	Highly significant
BD	1244.33	1	1244.33	374.42	<0.0001	V. highly significant
BE	5.18	1	5.18	1.56	0.2380	Nonsignificant
CD	123.77	1	123.77	37.24	<0.0001	V. highly significant
CE	5.625E-003	1	5.625E-003	1.693E-003	0.9679	Nonsignificant
DE	49.35	1	49.35	14.85	0.0027	Significant
Residual	36.56	11	3.32			
Pure error	0.068	5	0.014			
Corrected total	7962.78	31				

*SS:sum of squares; df:degree of freedom; MS:mean square.

also confirmed that within a low range of M : O, its increase reduced the transesterification efficiency, while vice versa occurred within a high range of M : O. The perturbation plots also proved the high sensitivity of the transesterification reaction towards the E–NH_2–Pr-SBA-15 nanobiocatalyst concentration, reaction temperature, and time. Moreover, the perturbation plots (Figure 7) presumptively indicated that, across the studied range, the transesterification efficiency was better at high and relatively low M : O molar ratio, high catalyst concentration, relatively high mixing rate, low-temperature, and time near to the center point.

The 2D contour plots and 3D RSM plots (Figure 8) elucidate the interactive effect of the studied parameters on the transesterification process. The elliptical shape (Figure 8(a)) of the possible statistical significant negative interactive effect of M : O and nanobiocatalyst concentration (p = 0.0177) indicated that the transesterification efficiency

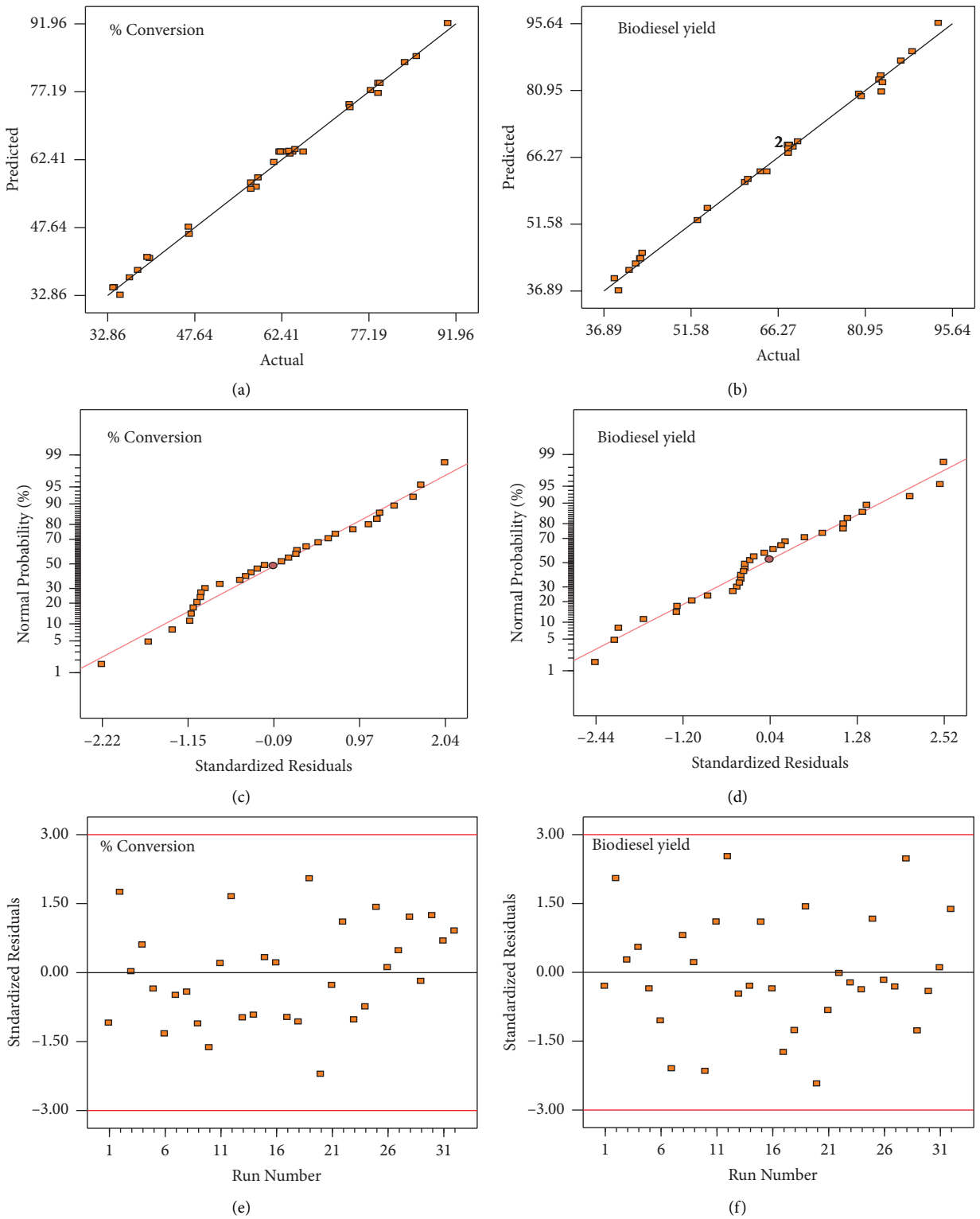

Figure 6: Diagnostic models' validation plots; predicted versus actual response (a, b), normal probability plots of residuals (c, d), and standardized residuals versus run numbers (e, f).

increased at low and high M : O (3 : 1 and 6 : 1) with the increase of nanobiocatalyst reaching its maximum at nine wt.% of E–NH_2–Pr-SBA-15.

The very high statistically significant negative interactive effect of M : O and reaction time ($p < 0.0001$) was pronounced in the 2D and 3D plots (Figure 8(b)). In contrast,

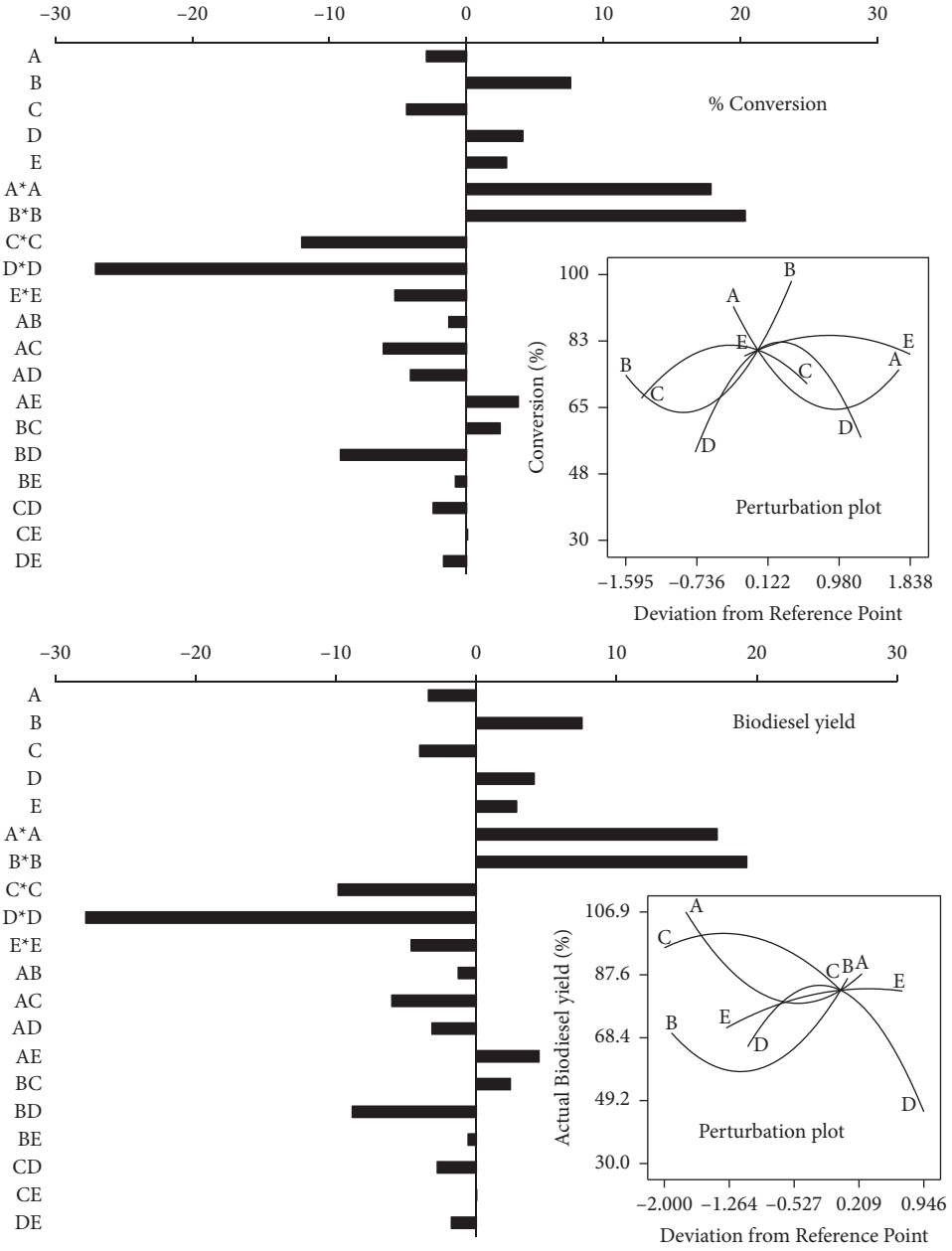

Figure 7: Pareto charts and perturbation plots representing the main and interactive effects of the studied parameters on the transesterification process.

the transesterification efficiency at low M : O (3 : 1) and high M : O (6 : 1) increased with the reaction time reaching its maximum within three *h* but decreased at a longer reaction time.

The inverted elliptical shape (Figure 8(c)) represents the highly statistically significant negative interactive effect of reaction time and temperature on the transesterification efficiency ($p = 0.0003$). The transesterification efficiency decreased at higher and longer reaction temperature and time (>50°C and three *h*, respectively) and was also low at lower and shorter reaction temperature and time (<50°C and three *h*, respectively).

Moreover, the statistically significant negative interactive effect of reaction time and mixing rate ($p = 0.0039$) on the transesterification efficiency (Figure 8(d)) indicated the decrease in % conversion at longer reaction time (>3 h). Nevertheless, it increased with the increase of mixing rate regardless of the reaction time, up to ≈450 rpm, and then slightly increased and/or remained nearly sustained at a higher mixing rate (>450 rpm).

The 2D and 3D plots of the interactive effect of M : O and reaction temperature and those of nanobiocatalyst concentration and reaction time pronounced their very high statistically significant adverse effects ($p < 0.0001$) onto the transesterification efficiency (Figure 8(e), 8(f)). It showed that at low M : O (<4.5 : 1), the biodiesel yield was recognizably increased with the increase in reaction temperature, but vice versa occurred at high M : O (>4.5 : 1). Moreover,

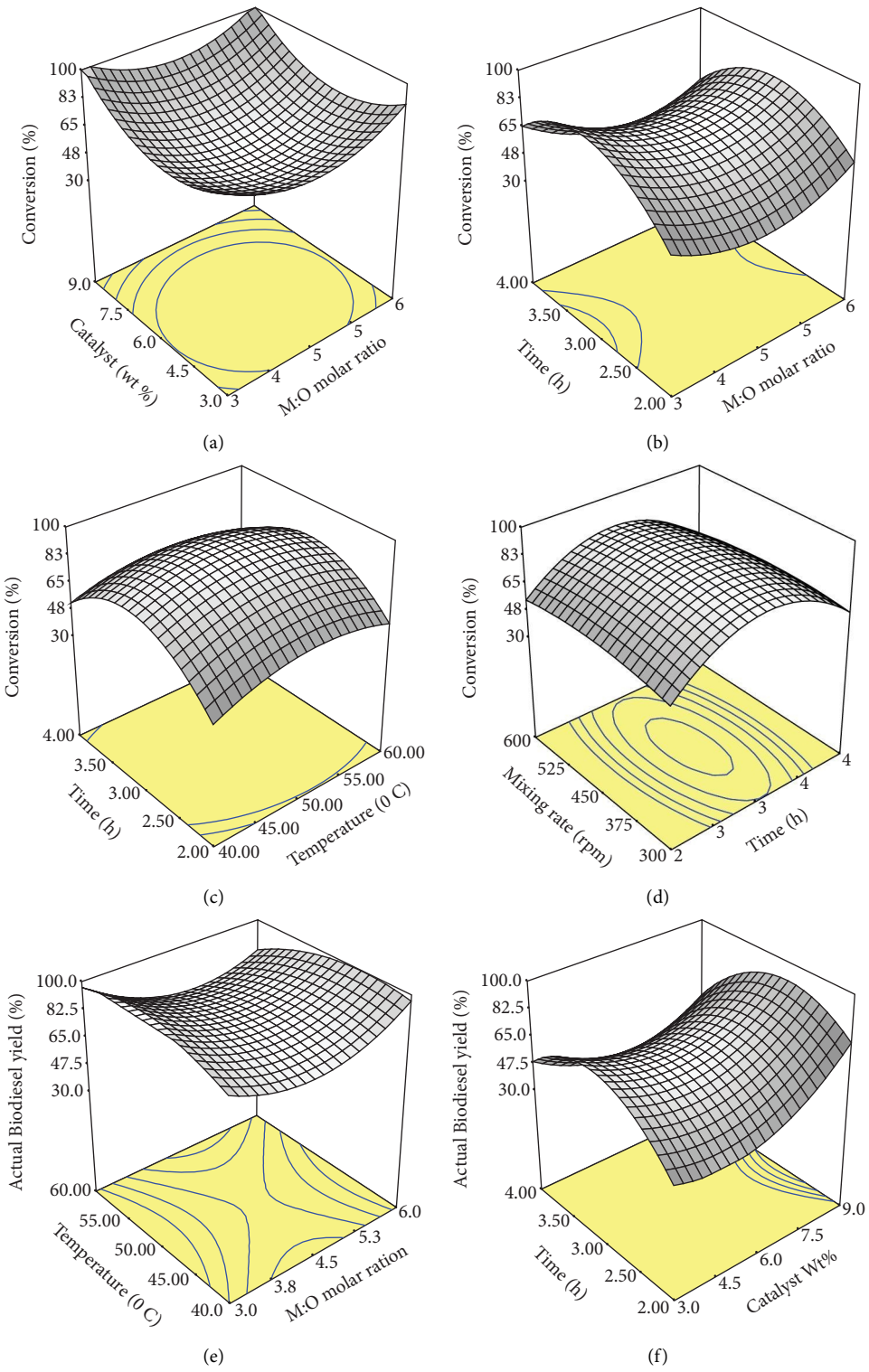

Figure 8: Continued.

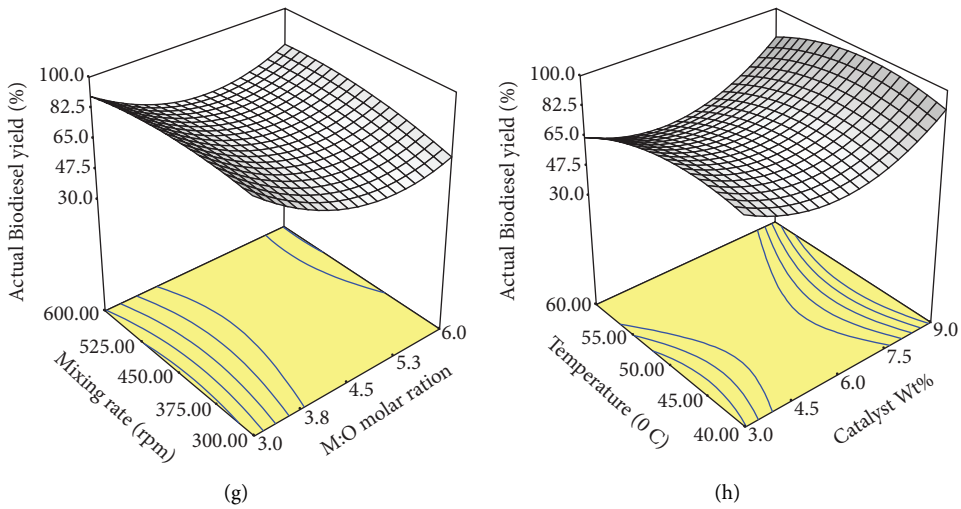

Figure 8: The 2D contour and 3D RSM plots representing the interactive effects of the studied independent parameters on the transesterification process.

the noticeable increase in the biodiesel yield with the increase in the nanobiocatalyst concentration decreased regardless of the catalyst concentration with a longer reaction time (>3 h).

Nevertheless, the exceptionally high statistically significant positive interactive effect of M : O and mixing rate on biodiesel yield was evident in the 3D plot (Figure 8(g), $p < 0.0001$). Regardless of the M : O molar ratio, the biodiesel yield increased with the increase of the mixing rate until reaching ≈450 rpm and then slightly increased and/or remained nearly sustained at a higher mixing rate (>450 rpm).

The high statistically significant positive interactive effect of nanobiocatalyst concentration and reaction temperature ($p = 0.0002$) was evident in the 3D plot (Figure 8(h)). Though, at low nanobiocatalyst concentration (3–4 wt.%), the biodiesel yield increased with the reaction temperature recording its maximum within (46–52°C). The same occurred at high catalyst concentration (8–9 wt.%), recording maximum biodiesel yield within high-temperature range (48–60°C).

The enhancement of the transesterification efficiency with the relatively higher mixing rate ≈450 rpm would indicate the possible elimination of mass transfer limitations and the manifestation of good mixing of the reactants. However, the decreased or sustained transesterification efficiency at a relatively higher mixing rate >450 rpm might be due to the possible occurrence of turbulence and increased mass transfer opposition. However, lipases are sensitive to high methanol concentrations and reaction temperature [18, 19, 24]. However, the prepared E-NH2-Pr-SBA-15 showed reasonably good tolerance to relatively elevated methanol concentration and process temperature, which adds to the advantages of immobilized PSP8 lipase E-NH2-Pr-SBA-15. That contradicted the observation reported by Shimada et al. [54]; where the immobilized *Candida Antarctica* lipase was inhibited at a high M : O (>1.5) molar ratio. It also contradicted the data reported by Arumugam and Ponnusami [32] for the immobilized *Candida Antarctica* lipase onto amino-functionalized SBA-15, where the biodiesel yield decreased at reaction temperature higher than 35°C. The increment of transesterification efficiency with relatively high reaction temperature might be, according to Ismail et al. [18]; due to the decrease in the viscosity of reaction mixture and the abolition of the mass transfer limitations. However, at higher elevated temperatures, denaturation of enzymes [32] and vaporization of methanol [18] might occur, consequently decreasing the transesterification efficiency. According to Nassar et al. [2] the elevated temperatures affect the methanol polarity, decreasing the available methoxide moieties required for commencing the transesterification reaction towards the forward direction producing the FAME.

The recorded sufficient transesterification efficiency over a wide range of the applied nanobiocatalyst concentrations also added to the advantages of the prepared E–NH_2–Pr-SBA-15 as it would indicate the non-agglomeration of the immobilized PSP8 lipase beads, the overwhelmed diffusion limitation, and the easiness of substrates reaching the active sites of the enzyme molecules, even at higher nanobiocatalyst concentrations. However, it was also noticed that the transesterification of WCO into biodiesel using the immobilized PSP8 lipase onto the NH_2-Pr-SBA-15 was mutually low at short and long reaction times. According to Ismail et al. [18]; that might be due to the initial time needed by the reactants to overcome the mass transfer limitation and get in contact with the active sites of the enzyme molecules. Nevertheless, according to Yang et al. [55] and Mohammadi et al. [37]; the production and accumulation of the oil insoluble hydrophilic glycerol with the transesterification progressive reaction time (Scheme 1), would straightforwardly adsorb onto the immobilized lipase surface active sites, negatively affect the enzyme activity and operating constancy and consequently the transesterification reaction. Moreover, according to Nassar et al. [2]; the accumulated glycerol

Table 3: The predicted optimum operating for the transesterification of WCO with methanol in the presence of the prepared E–NH_2–Pr-SBA-15.

No.	M : O molar ratio	Immobilized enzyme wt.%	Temp. °C	Time *h*	Mixing rate rpm	Desirability	% conversion		Percentage error	StD			Percentage error	StD
							Predicted	Actual			Predicted	Actual		
1	3.07	8.58	59.09	3.21	314.09	1.000	94.6016	95.4	0.83	1.093	101.3	98	−3.4	0.574
2	5.79	8.61	50.81	2.86	541.45	1.000	97.1337	96.6	−0.55		100.8	97	−3.9	
3	3.04	8.77	47.71	2.92	319.14	1.000	104.694	97.5	−7.4		109.3	98	−11.5	
4	3.12	3.08	48.60	3.19	495.53	1.000	94.4065	97.85	3.52		97.7	97.01	−0.71	

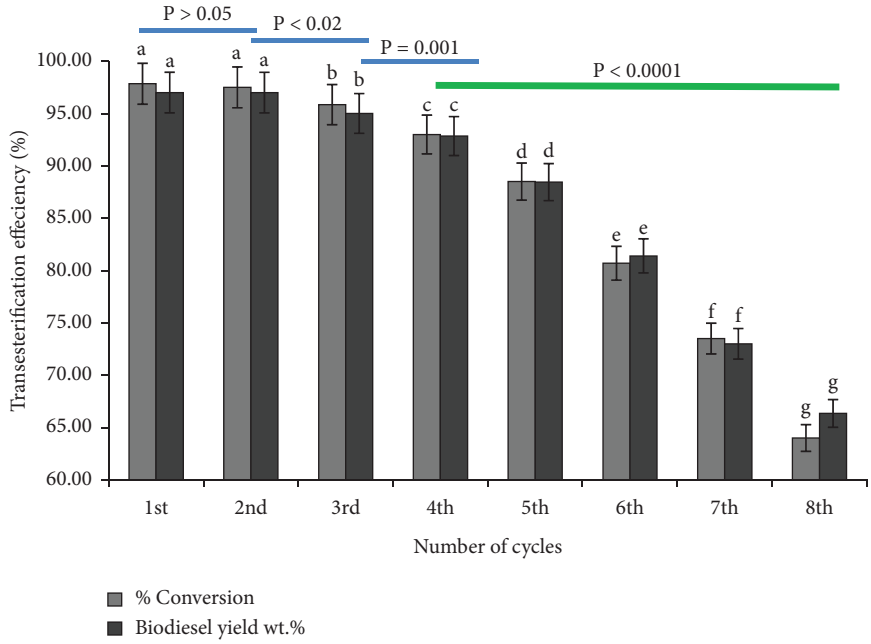

Figure 9: Reusability of the immobilized PSP8 lipase E–NH_2–Pr-SBA-15.

would dissolve in the unreacted methanol, shifting the transesterification process backward to the reverse direction, lowering the biodiesel yield.

3.7. Statistical Optimization of the Transesterification Process. The Design-Expert software, version 6.0.7, was applied to optimize the operating conditions to achieve the maximum transesterification efficiency. The desired goal for each operational condition (M : O, E–NH_2–Pr-SBA-15 concentration, reaction time, reaction temperature, and mixing rate) was chosen "within" the studied range, and the responses (% conversion and biodiesel yield wt.%) were defined as maximum. Additional experiments were then performed applying the predicted optimum conditions listed in (Table 3). The desirability function value for those optimum conditions was found to be 1.000. The results of the laboratory experiments agreed well with the predicted response values. The standard deviation (StD) and percentage error were calculated for the experimental validation, recording approximately 1.093 and 3.08% for the % conversion, while 0.574 and 4.88% for biodiesel yield, respectively. That indicated the process optimization by FCCD of experiments was capable and reliable to optimize the batch transesterification reaction of WCO with methanol using the immobilized E–NH_2–Pr-SBA-15.

From the economic point of view of decreasing time, energy, methanol, enzyme, and nanobiocatalyst consumption, the optimum operating conditions were chosen to be 3.12 : 1 M : O, 3.08 wt.% E–NH_2–Pr-SBA-15, 48.6 °C, 3.19 h, and 495.53 rpm.

3.8. Reusability and Feasibility of the Prepared E–NH_2–Pr-SBA-15. The reusability of the prepared nanobiocatalyst under the predicted optimum conditions was examined. The transesterification efficiency over eight successive cycles is illustrated in Figure 9, which proved that E–NH_2–Pr-SBA-15 had been used for two successive cycles without a decrease in its activity ($p > 0.05$ at $\alpha = 0.05$ level, 95% confidence interval). Moreover, there was no noteworthy decrease in E–NH_2–Pr-SBA-15 activity after three successive cycles ($p = 0.001$ at $\alpha = 0.05$ level, 95% confidence interval). The prepared E–NH_2–Pr-SBA-15 kept approximately 96%, 75%, and 68% of its initial activity after four, seven, and eight successive cycles ($p < 0.0001$ at $\alpha = 0.05$ level, 95% confidence interval). That ascertained its operational flexibility, easy separation, stability, and long lifetime, which reinforce the recommended commercial application of E–NH_2–Pr-SBA-15 for the valorization of WCO into biodiesel, whatever on continuous or batch industrial scale.

The *Bacillus stratosphericus PSP8* lipase immobilized amine-functionalized SBA-15 expressed a comparable transesterification activity relative to the previously published literature (Table 4) at a one-step methanol feeding process without the need of any co-solvents. The comparatively large biodiesel yield obtained using the *Bacillus stratosphericus* PSP8 lipase immobilized amine-functionalized SBA-15 within a quite short-time and mild temperature transesterification process. Besides, a relatively low alcohol and nanobiocatalyst consumption would, according to Nassar et al. [2]; indicate the dimensioned mass transfer limitations which usually occur in the heterogeneously catalyzed biodiesel production processes. That adds to the advantages of the applied *Bacillus stratosphericus* PSP8 lipase immobilized amine-functionalized SBA-15. However, the recorded loss of activity (≈9%–32%) within the 5^{th} to the 8^{th} cycles may be ascribed to; the possible conformational changes of PSP8 lipase, the blocking of the active lipase sites, or the gradual loss of the bounded lipase during the reaction procedures [23], the lipase leaching [43], and/or enzyme denaturation [21].

Table 4: Comparative study between the transesterification activity of E–NH_2–Pr-SBA-15 and the previously published lipase immobilized SBA-15.

Nanobiocatalyst	Conditions	Transesterification efficiency and reusability	References
Candida Antarctica lipase immobilized on amine-functionalized SBA-15	*Calophyllum inophyllum* linn oil, 6 : 1 M : O, 6.25 wt.% nanobiocatalyst, 35°C, 100 rpm, 6 h n-hexane and water as cosolvents	94% FAME yield lost ≈15% of its initial activity after 10 cycles	Arumugam and Ponnusami [32]
Rhizomucor miehei lipase covalently immobilized on aldehyde-functionalized SBA-15	Colza oil, 3 : 1 M : O, 2.27 wt.% nanobiocatalyst, 50°C, 250 rpm, 72 h t-butanol as co-solvent 3-Stepwise methanol	99% conversion retained 74% of its initial activity after 4 cycles	Mohammadi et al. [37]
Candida Antarctica lipase, *Thermomyces lanuginosus* lipase, and *Rhizomucor miehei* lipase covalently immobilized on SBA-epoxy	Canola oil, 3 : 1 M : O, 3.8 wt.% nanobiocatalyst, 50°C, 250 rpm, 72 h t-butanol and water as cosolvents 3-stepwise methanol feeding	61% conversion, 14 cycles 98.6% conversion, 20 cycles 95% conversion, 7 cycles	Babaki et al. [38]
Porcine pancreatic lipase covalently immobilized on glutaraldehyde chemically modified amine-functionalized SBA-15	*Castor* oil, 20.25 wt.% methanol, 25 wt.% nanobiocatalyst, 42°C, 250 rpm n-hexane and water as cosolvents	88.6% FAME yield	Davoodimehr et al. [39]
Candida rugosa lipase physically adsorbed on SBA-15	Cotton seed oil, 6 : 1 M : O, 5 wt.% nanobiocatalyst, 40°C, 68 h 3-stepwise methanol feeding	98% FAME yield Lost 54% of its initial activity in the 2nd cycle	Katiyar et al. [21]
Burkholderia cepacia lipase physically adsorbed on SBA-15	Palm kernel oil, 6 : 1 ethanol:oil, 10 wt.% nanobiocatalyst, 45°C, 150 rpm, 72 h	>90% biodiesel yield 98.9% conversion retained 90% of its initial activity after 5 cycles	Pinto et al. [36]
Bacillus stratosphericus PSP8 lipase immobilized on amine-functionalized SBA-15	Waste cooking oil, 3.12 : 1 M : O, 3.08 wt.% nanobiocatalyst, 48.6°C, 3.19 h, 495.53 rpm without any cosolvents One-step methanol feeding	97.85% conversion 97.01% biodiesel yield 4 cycles without significant loss in activity retained 68% % of its initial activity after 8 cycles	This study

3.9. Physicochemical Characterization of the Produced Biodiesel. The produced biodiesel met the international biodiesel standard specifications JUS [56, 57] (Table 5). Thus, it can be ranked as a realistic fuel to be applied as a substitute and/or complementary to petro-diesel. The drop in the values of biodiesel TAN, density, and viscosity relative to those of the WCO by 89.12, 4.08, and 92.4%, respectively, confirmed the excellent transesterification efficiency. The iodine value, a measure of unsaturation degree, dramatically influences the fuel oxidation tendency and stability [2]. The I_2 value of the produced biodiesel was recorded at 110 mg I_2/100 g oil and agreed well with the EN14214 standards (<120 mg I_2/100 g oil). The acid value indicates the content of free fatty acids (FFAs) in the sample and influences fuel aging [18]. The acid value of the produced biodiesel recorded 0.31 mg KOH/g oil and agreed well with the international biodiesel standards (<0.5 mg KOH/g oil). Thus, no operational problems, such as corrosion and pump plugging, would occur.

The relatively good cold flow characteristics, with a cloud point of 3°C and a pour point of 9°C (Table 5), might be ascribed to the high unsaturated FAME content of the produced biodiesel (≈64.5%) and recommend its application in cold weather. Not only that, but good flow properties also characterized the produced biodiesel; density of 0.8893 g/cm^3 and viscosity of 3.7 cSt and rational values of specific gravity and API, recording 0.8862 and 26.32, respectively. Although the produced biodiesel has a lower CV~39.381 MJ/kg than that of the Egyptian petro-diesel standards, it is higher than that of the biodiesel standards.

Moreover, the produced biodiesel was characterized by four significant advantages (Table 5); it has no sulfur, so it meets the goal of the petroleum industry for ultra-low to zero-sulfur-diesel; and its burning would not emit sulfur oxides, triggering engine corrosion, air pollution, and acid rain. The produced biodiesel had a relatively high flash point of 155°C. So, it is much less flammable than conventional petro-diesel, and hence, it is much safer in usage, storing, and transference. In addition, the viscosity of the produced biodiesel was 3.7 cSt, which is competitive with that of conventional petro-diesel. Hence, no hardware or engine amendments would be needed to apply the produced biodiesel to the market. The distillation temperatures (DTs) characterize the volatility of the fuel and have a significant effect on the burning efficiency of the diesel engine [18]. The fairly observed high DTs for the produced biodiesel (Table 5) would reduce the ignition delay of the fuel and minimize the possibility of knocking in the diesel engine.

Table 5: The physicochemical characteristics of the produced biodiesel compared to the international biodiesel standards and Egyptian petro-diesel standard specifications.

Physicochemical characteristics	Unit	Biodiesel sample	Egyptian petro-diesel standards	European biodiesel JUS EN14214	American biodiesel ASTM D-6751
Density @ 15.56°C	g/cm^3	0.8893	0.82–0.87	0.86–0.9	—
Specific gravity		0.8862	—	—	—
API		26.32	—	—	—
Kinematic viscosity @ 40°C	cSt	3.7	1.6–1.7	3.5–5	1.9–6
Cloud point	°C	−3	—	−4	—
Pour point	°C	−9	4.5	—	—
Calorific value	MJ/kg	39.381	>44.3	32.9	
Flash point	°C	155	>55	>101	>130
Total sulfur	wt.%	Nil	<1.2	<0.01	<0.05
TAN	mg KOH/g oil	0.31	Nil	<0.5	<0.5
Iodine number	mg I_2/100 g oil	110	—	<120	—
Distillation profile					
Initial boiling point		215			
10 ml		256			
20 ml		273			
30 ml		289			
40 ml		305			
50 ml	°C	320			
60 ml		327			
70 ml		332			
80 ml		339			
90 ml		347			
96 ml		351			
Recovery	%	96	90% recovered 282–338°C		90% recovered <360°C
Residue	%	2			
Loss	%	2			

4. Conclusion

The valorization of WCO into eco-friendly biodiesel using sustainable immobilized lipase enzymes has positive impacts on the dilemma of food versus fuel, waste management, climate change, and the depletion of renewable energy resources. Most of the published immobilized lipase/SBA-15 catalyzed transesterification processes used nonedible oil or standard fatty acids to produce biodiesel. Thus, as far as our knowledge, this is the first time to apply *Bacillus stratosphericus* PSP8 lipase immobilized onto amine-functionalized SBA-15 (E–NH_2–Pr-SBA-15) to valorize WCO into highly qualified biodiesel in the absence of any co-solvent. Furthermore, the statistical optimization of the transesterification process using RSM based on FCCCD proved to be very suitable for maximizing the production yield of highly qualified eco-friendly biodiesel. The produced E–NH_2–Pr-SBA-15 proved to have many advantages; it had a large biodiesel yield throughout a relatively mild transesterification operational process, in addition to low alcohol and enzyme consumption. Furthermore, the high purity of the obtained biodiesel without the need for a washing step, usually applied in a homogenous transesterification reaction, would decrease the water consumption in the biodiesel industry. E–NH_2–Pr-SBA-15 is also characterized by a long lifetime, sufficient operational stability, and reusability, which add to its feasibility and recommend its application in continuous industrial-scale processes.

Data Availability

Data are available on request.

Disclosure

Abdallah R. Ismail and Hamdy Kashtoh are co-first authors.

Conflicts of Interest

The authors declare they have no conflicts of interest.

Authors' Contributions

The authors Abdallah R. Ismail and Hamdy Kashtoh have contributed equally to this work.

Acknowledgments

This research was supported by the Basic Science Research Program through the National Research Foundation of Korea (NRF) and funded by the Ministry of Education (NRF-2021R1F1A1060297).

References

[1] T. A. Degfie, T. T. Mamo, and Y. S. Mekonnen, "Optimized biodiesel production from waste cooking oil (WCO) using calcium oxide (CaO) nanocatalyst," *Scientific Reports*, vol. 9, no. 1, Article ID 18982, 2019.

[2] H. N. Nassar, A. R. Ismail, R. A. El-Salamony, O. Aboelazayem, S. A. Abu Amr, and N. S. El-Gendy, "Animal bone affluence in environmental reclamation:biodiesel production, petro-diesel biodesulfurization and wastewater photo-treatment," *Biofuels, Bioprod. Bioref.*vol. 15, no. 3, pp. 770–792, 2021.

[3] H. K. Jeswani, A. Chilvers, and A. Azapagic, "Environmental sustainability of biofuels:a review," *Proc. R. Soc. A*, vol. 476, no. 2243, Article ID 20200351, 2020.

[4] N. S. El-Gendy, S. F. Deriase, and A. Hamdy, "The optimization of biodiesel production from waste frying corn oil using snails shells as a catalyst," *Energy Sources, Part A:Recovery, Utilization, and Environmental Effects*, vol. 36, no. 6, pp. 623–637, 2014.

[5] H. I. Hamouda, H. N. Nassar, H. R. Madian, M. H. El-Sayed, A. A. El-Ghamry, and N. S. El-Gendy, "Isolation of fermentative microbial isolates from sugar cane and beet molasses and evaluation for enhanced production of bioethanol," *Energy Sources, Part A:Recovery, Utilization, and Environmental Effects*, vol. 38, no. 15, pp. 2170–2180, 2016.

[6] J. Yang, Z. Xin, Q. S. He, K. Corscadden, and H. Niu, "An overview on performance characteristics of bio-jet fuels," *Fuel*, vol. 237, pp. 916–936, 2019.

[7] S. Achinas, V. Achinas, and G. J. W. Euverink, "A technological overview of biogas production from biowaste," *Engineering*, vol. 3, pp. 299–307, 2017.

[8] O. Aboelazayem, N. S. El-Gendy, A. A. Abdel-Rehim, F. Ashour, and M. A. Sadek, "Biodiesel production from castor oil in Egypt:process optimisation, kinetic study, diesel engine performance and exhaust emissions analysis," *Energy*, vol. 157, pp. 843–852, 2018.

[9] A. Avinash, P. Sasikumar, and A. Murugesan, "Understanding the interaction among the barriers of biodiesel production from waste cooking oil in India- an interpretive structural modeling approach," *Renewable Energy*, vol. 127, pp. 678–684, 2018.

[10] F. Fangfang, A. Alagumalai, and O. Mahian, "Sustainable biodiesel production from waste cooking oil:ANN modeling and environmental factor assessment," *Sustainable Energy Technologies and Assessments*, vol. 46, Article ID 101265, 2021.

[11] N. S. El-Gendy, B. A. Ali, SS. Abu Amr, H. A. Aziz, and A. S. Mohamed, "Application of D-optimal design and RSM to optimize the transesterification of waste cooking oil using natural and chemical heterogeneous catalyst," *Energy Sources, Part A:Recovery, Utilization, and Environmental Effects*, vol. 38, no. 13, pp. 1852–1866, 2016.

[12] Y. H. Tan, M. O. Abdullah, J. Kansedo, N. M. Mubarak, Y. S. Chan, and C. Nolasco-Hipolito, "Biodiesel production from used cooking oil using green solid catalyst derived from calcined fusion waste chicken and fish bones," *Renewable Energy*, vol. 139, pp. 696–706, 2019.

[13] A. Avinash and A. Murugesan, "Economic analysis of biodiesel production from waste cooking oil," *Energy Sources, Part B:Economics, Planning and Policy*, vol. 12, no. 10, pp. 890–894, 2017.

[14] A. Demirbas, "Bio-diesel from waste cooking oil via base-catalytic and supercritical methanol transesterification," *Energy Conversion and Management*, vol. 50, no. 4, pp. 923–927, 2009.

[15] Y. S. Erchamo, T. T. Mamo, G. A. Workneh, and Y. S. Mekonnen, "Improved biodiesel production from waste cooking oil with mixed methanol–ethanol using enhanced eggshell-derived CaO nano-catalyst," *Scientific Reports*, vol. 11, no. 1, p. 6708, 2021.

[16] F. Bueso, L. Moreno, M. Cedeño, and K. Manzanarez, "Lipase-catalyzed biodiesel production and quality with *Jatropha curcas* oil:exploring its potential for Central America," *Journal of Biological Engineering*, vol. 9, no. 1, p. 12, 2015.

[17] N. S. El-Gendy, A. Hamdy, and S. S. Abu Amr, "Application of D-optimal design and RSM to optimize the transesterification of waste cooking oil using a biocatalyst derived from waste animal bones and Novozym 435," *Energy Sources, Part A: Recovery, Utilization, and Environmental Effects*, vol. 37, no. 11, pp. 1233–1251, 2015.

[18] A. R. Ismail, S. B. El-Henawy, M. A. Betiha et al., "Optimization of batch Novozym435-catalyzed transesterification of waste cooking oil with methanol for biodiesel production in a solvent-free medium," *Energy Sources, Part A:Recovery, Utilization, and Environmental Effects*, vol. 39, no. 9, pp. 911–925, 2017.

[19] Y. X. Li and B. X. Dong, "Optimization of lipase-catalyzed transesterification of cotton seed oil for biodiesel production using response surface methodology," *Brazilian Archives of Biology and Technology*, vol. 59, no. 0, Article ID e161503571, 2016.

[20] S. Imanparast, M. A. Faramarzi, and J. Hamedi, "Production of a *Cyanobacterium*-based biodiesel by the heterogeneous biocatalyst of SBA-15@oleate@lipase," *Fuel*, vol. 279, Article ID 118580, 2020.

[21] M. Katiyar, K. Abida, and A. Ali, "*Candida rugosa* lipase immobilization over SBA-15 to prepare solid biocatalyst for cotton seed oil transesterification," *Materials Today Proceedings*, vol. 36, pp. 763–768, 2021.

[22] J. Gao, L. Shi, Y. Jiang, L. Zhou, and Y. He, "Formation of lipase *Candida* sp. 99-125 CLEAs in mesoporous silica: characterization and catalytic properties," *Catalysis Science & Technology*, vol. 3, no. 12, pp. 3353–3359, 2013.

[23] M. Karimi, "Immobilization of lipase onto mesoporous magnetic nanoparticles for enzymatic synthesis of biodiesel," *Biocatalysis and Agricultural Biotechnology*, vol. 8, pp. 182–188, 2016.

[24] O. Kãse, M. Tüter, and H. A. Aksoy, "Immobilized *Candida antarctica* lipase-catalyzed alcoholysis of cotton seed oil in a solvent-free medium," *Bioresource Technology*, vol. 83, no. 2, pp. 125–129, 2002.

[25] J. H. Lee, J. H. Lee, D. S. Kim, H. Y. Yoo, C. Park, and S. W. Kim, "Biodiesel production by lipases co-immobilized on the functionalized activated carbon," *Bioresource Technology Reports*, vol. 7, Article ID 100248, 2019.

[26] Y. Li, W. Wang, and P. Han, "Immobilization of *Candida* sp 99-125 lipase onto silanized SBA-15 mesoporous materials by physical adsorption," *Korean Journal of Chemical Engineering*, vol. 31, no. 1, pp. 98–103, 2014.

[27] T. Tan, J. Lu, K. Nie, L. Deng, and F. Wang, "Biodiesel production with immobilized lipase:a review," *Biotechnology Advances*, vol. 28, no. 5, pp. 628–634, 2010.

[28] N. H. Abdallah, M. Schlumpberger, D. A. Gaffney, J. P. Hanrahan, J. M. Tobin, and E. Magner, "Comparison of mesoporous silicate supports for the immobilisation and activity of cytochrome c and lipase," *Journal of Molecular Catalysis B:Enzymatic*, vol. 108, pp. 82–88, 2014.

[29] E. Magner, "Immobilisation of enzymes on mesoporous silicate materials," *Chemical Society Reviews*, vol. 42, no. 15, pp. 6213–6222, 2013.

[30] S. i Matsuura, M. Chiba, T. Tsunoda, and A. Yamaguchi, "Enzyme immobilization in mesoporous silica for enhancement of thermostability," *Journal of Nanoscience and Nanotechnology*, vol. 18, no. 1, pp. 104–109, 2018.

[31] A. Arumugam and V. Ponnusami, "Synthesis of SBA-15 from low cost silica precursor obtained from sugarcane leaf ash and its application as a support matrix for lipase in biodiesel production," *Journal of Sol-Gel Science and Technology*, vol. 67, no. 2, pp. 244–250, 2013.

[32] A. Arumugam and V. Ponnusami, "Enzymatic transesterification of *Calophyllum inophyllum* oil by lipase immobilized on functionalized SBA-15 synthesized from low-cost precursor," *Biomass Conv Bioref*, vol. 4, no. 1, pp. 35–41, 2014.

[33] G. O. Ferrero, E. M. Sánchez-Faba, and G. A. Eimer, "Two Products one catalyst:emulsifiers and biodiesel production combining enzymology, nanostructured materials engineering and simulation models," *Chemical Engineering Journal*, vol. 348, pp. 960–965, 2018.

[34] H. Gustafsson, E. M. Johansson, A. Barrabino, M. Odén, and K. Holmberg, "Immobilization of lipase from *Mucor miehei* and *Rhizopus oryzae* into mesoporous silica - the effect of varied particle size and morphology," *Colloids and Surfaces B: Biointerfaces*, vol. 100, pp. 22–30, 2012.

[35] C. Carteret, J. Jacoby, and J. L. Blin, "Using Factorial experimental design to optimize biocatalytic biodiesel production from *Mucor miehei* lipase immobilized onto ordered mesoporous materials," *Microporous and Mesoporous Materials*, vol. 268, pp. 39–45, 2018.

[36] F. Pinto, F. R. Fernandes, V. P. S. Caldeira et al., "Influence of the procedure to immobilize lipase on SBA-15 for biodiesel production from palm kernel oil," *Catalysis Letters*, vol. 151, pp. 2187–2196, 2021.

[37] M. Mohammadi, M. Ashjari, S. Dezvarei, M. Yousefi, M. Babaki, and J. Mohammadi, "Rapid and high-density covalent immobilization of *Rhizomucor miehei* lipase using a multi component reaction:application in biodiesel production," *RSC Advances*, vol. 5, no. 41, pp. 32698–32705, 2015.

[38] M. Babaki, M. Yousefi, Z. Habibi et al., "Enzymatic production of biodiesel using lipases immobilized on silica nanoparticles as highly reusable biocatalysts:effect of water, *t*-butanol and blue silica gel contents," *Renewable Energy*, vol. 91, pp. 196–206, 2016.

[39] A. Davoodimehr, T. Nematian, A. Shakeri, and N. Ghaemi, "Biodiesel Production from castor Oil in the Presence of Lipase/functionalized Mesoporous SBA-15," 2021, https://www.researchgate.net/publication/351046127_Biodiesel_Production_from_Castor_oil_in_the_Presence_of_Lipase_Functionalized_Mesoporous_SBA-15.

[40] P. Shah, N. Sridevi, A. Prabhune, and V. Ramaswamy, "Structural features of *Penicillin acylase* adsorption on APTES functionalized SBA-15," *Microporous and Mesoporous Materials*, vol. 116, no. 1-3, pp. 157–165, 2008.

[41] H. Zhu, R. Maheswari, A. Ramanathan, and B. Subramaniam, "Evaporation-induced self-assembly of mesoporous zirconium silicates with tunable acidity and facile catalytic dehydration activity," *Microporous and Mesoporous Materials*, vol. 223, pp. 46–52, 2016.

[42] L. D. Castro-Ochoa, C. Rodríguez-Gómez, G. Valerio-Alfaro, and R. Oliart Ros, "Screening, purification and characterization of the thermoalkalophilic lipase produced by *Bacillus thermoleovorans* CCR11," *Enzyme and Microbial Technology*, vol. 37, no. 6, pp. 648–654, 2005.

[43] J. Gao, Y. Jiang, J. Lu, Z. Han, J. Deng, and Y. Chen, "Dopamine-functionalized mesoporous onion-like silica as a new matrix for immobilization of lipase *Candida* sp. 99–125," *Scientific Reports*, vol. 7, no. 1, Article ID 40395, 2017.

[44] American Society for Testing and Materials (Astm), *Annual Book of ASTM Standards. Petroleum products and lubricants (I–III)*, West Conshohocken, PA, 2010.

[45] J. Sun, Y. Chen, J. Sheng, and M. Sun, "Immobilization of *Yarrowia lipolytica* lipase on macroporous resin using different methods:characterization of the biocatalysts in hydrolysis reaction," *BioMed Research International*, vol. 2015, pp. 1–7, 2015.

[46] M. Kou, S. Feng, and N. Zhong, "Immobilization of lecitase® ultra onto the amino-functionalized SBA-15 and their applications in glycerolysis," *Journal of Oleo Science*, vol. 69, no. 4, pp. 347–358, 2020.

[47] H. Veisi, A. Naeimi, B. Maleki, S. S. Ashrafi, and A. Sedrpoushan, "Synthesis of 5-Alkylidene-2, 4-thiazolidinediones and rhodanines promoted by propylamino-functionalized nano-structured SBA-15," *Organic Preparations and Procedures International*, vol. 47, no. 4, pp. 309–315, 2015.

[48] X. Wang, Y. Zhang, W. Luo et al., "Synthesis of ordered mesoporous silica with tunable morphologies and pore sizes via a nonpolar solvent-assisted stober method," *Chemistry of Materials*, vol. 28, no. 7, pp. 2356–2362, 2016.

[49] P. Sharma and A. Sinph, "Phosphine free SBA-15-EDTA-Pd highly active recyclable catalyst:synthesis, characterization and application of Suzuki and Sonogashira reaction," *Catal Sienc Technnol*, vol. 4, pp. 2978–2989, 2014.

[50] Z. J. Farsangi, A. Beitollahi, B. Hatton et al., "One-pot controllable synthesis of carboxylic group functionalized hollow mesoporous silica nanospheres with efficient cisplatin delivery," *RSC Advances*, vol. 6, pp. 67592–67598, 2016.

[51] H. M. Salvi and G. D. Yadav, "Surface functionalization of SBA-15 for immobilization of lipase and its application in synthesis of alkyl levulinates:optimization and kinetics," *Biocatalysis and Agricultural Biotechnology*, vol. 18, Article ID 101038, 2019.

[52] M. A. Betiha, M. F. Menoufy, A. M. Al-Sabagh, H. M. Hassan, and S. A. Mahoud, "Acidic mesostructured aluminosilicates assembled from economic acidic template characterized by catalytic cracking reaction," *Microporous and Mesoporous Materials*, vol. 204, pp. 15–24, 2015.

[53] A. Badiei, H. Goldooz, and G. M. Ziarani, "A novel method for preparation of 8-hydroxyquinoline functionalized mesoporous silica:aluminum complexes and photoluminescence studies," *Applied Surface Science*, vol. 257, no. 11, pp. 4912–4918, 2011.

[54] Y. Shimada, Y. Watanabe, A. Sugihara, and Y. Tominaga, "Enzymatic alcoholysis for biodiesel fuel production and application of the reaction to oil processing," *Journal of Molecular Catalysis B:Enzymatic*, vol. 17, no. 3-5, pp. 133–142, 2002.

[55] Y. Gao, T. Tan, K. Nie, and F. Wang, "Immobilization of lipase on macroporous resin and its application in synthesis of biodiesel in low aqueous media," *Chinese Journal of Biotechnology*, vol. 22, no. 1, pp. 114–118, 2006.

[56] American Society for Testing and Materials (ASTM) D-6751-15ce1, *Standard Specification for Bio-Diesel Fuel (B100) Blend Stock for Distillate Fuels*, American Society for Testing Materials, West Conshohocken, PA, 2008.

[57] J. U. S. En14214, *Automotive Fuels. Fatty Acid Methyl Esters (FAME) for Diesel Engines- Requirements and Test Methods*, Standardization Institute, Belgrade, Serbia, 2004.